Unexpected ultrafast and high adsorption capacity of oxygen vacancy-rich WO_x/C nanowire networks for aqueous Pb^{2+} and methylene blue removal

Shouwei Zhang,†[a,c,d] Hongcen Yang,†[a] Huiyan Huang,[b] Huihui Gao,[a] Ruya Cao,[a] Xiangxue Wang,[d] Jiaxing Li,[c,d]* Xijin Xu,[a]* Xiangke Wang[d]*

[a]School of Physics and Technology, University of Jinan, Shandong, 250022, P. R. China. *E-mail: sps_xuxj@ujn.edu.cn

[b]School of Chemical and Environmental Engineering, Wuyi University, Jiangmen 529020, China.

[c]Institute of Plasma Physics, Chinese Academy of Sciences P.O. Box 1126, 230031 Hefei, P. R. China Tel: +86-551-65596617, Fax: +86-551-65591310, *E-mail: lijx@ipp.ac.cn(J. Li)

[d]School of Environmental Science and Engineering, North China Electric Power University, Beijing 102206, PR China *E-mail: xkwang@ncepu.edu.cn

†These authors contributed equally to this work.

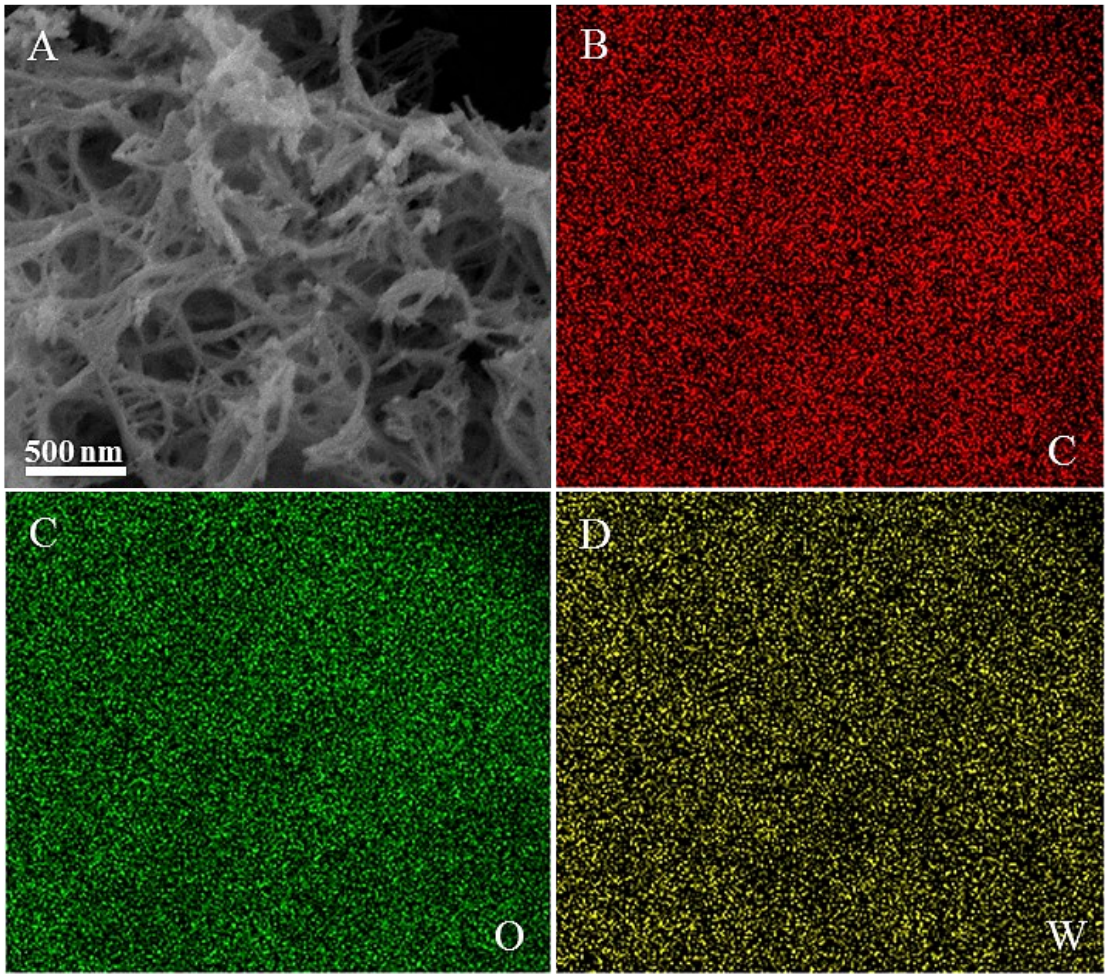

Figure S1. The element mapping of W, O and C of WO_x/C nanowire networks.

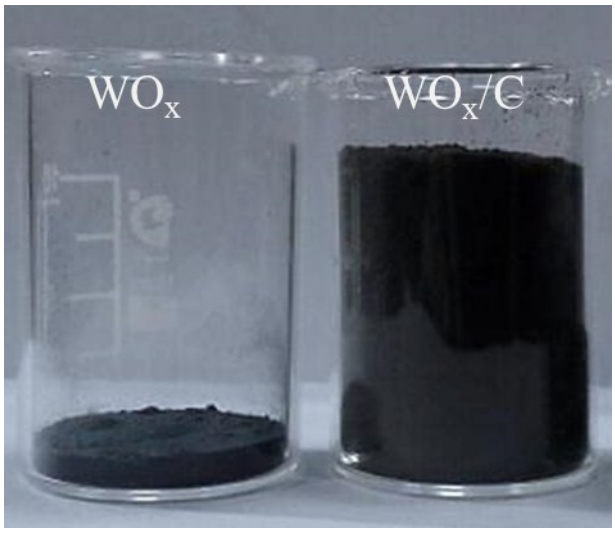

Figure S2. Photo of WO_x and WO_x/C nanowire networks from one batch process.

The adsorption behaviors of MO (anionic dyes) on WO_x@C networks were investigated. The maximum capacities based on the experiment data were ~1188.3 mg/g for MB and 154.1 mg/g for MO, respectively. The different adsorption behaviors of MB (cationic dyes) and MO (anionic dyes) on WO_x@C are due to the fact that they carry opposite charges. Zeta potential results indicated that WOx@C nanowire networks are negative over the entire pH range from ~2.0 to 12.0, and thus can more effectively capture positively charged dyes by electrostatic attraction.

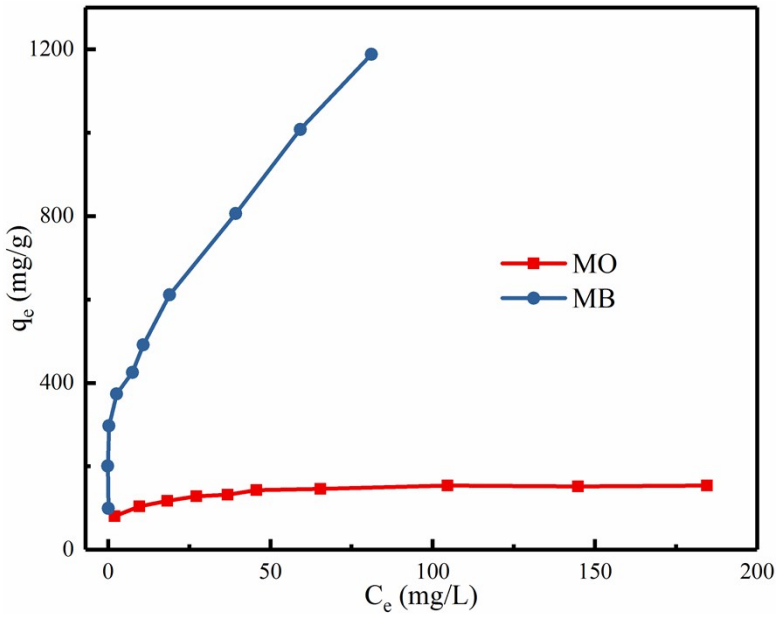

Figure S3. Adsorption isotherms of MB and MO on WOx@C nanowire networks.

The reusability is a key factor for an adsorbent and Figure S4 indicated the cycle performance of the WO_x/C nanowire networks toward MB adsorption. After 5cycles, the MB removal efficiency changes from ~99.7% to 94.3%. Namely, the adsorption capacity of WO_x/C networks for MB decrease slowly with increasing cycle number. Such a decrease is unavoidable due to the wastage of the adsorbent during each cycle. Therefore, the excellent stability makes the fabricated WO_x/C nanowire networks a perfect candidate for environment remediation.

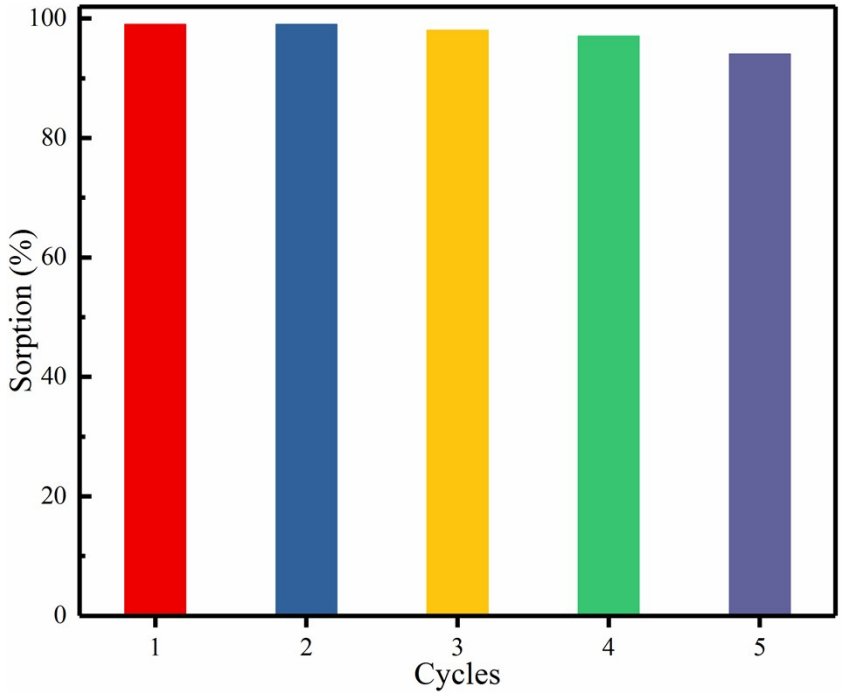

Figure S4. The recycle performance of WO_x/C networks toward 80 mg/L MB solution.

The pH value of the solution had a significant influence on theadsorption of Pb^{2+} on the WO_x/C networks. The uptake of Pb^{2+} increased with increasing pH values (see Figure S5A). The surface of WO_x/C networks is negatively charged and thus can capture positively charged pollutants by electrostatic attraction. According to the zeta-potential results, the surface charge on WO_x/C is larger at higher pH values, which results in enhancement of the electrostatic attraction between WO_x/C and Pb^{2+}ions. In addition, the number of available adsorption sites on the WO_x/C increased at higher pH values due to deprotonation. Therefore, higher pH values are favorable for adsorption removal of Pb^{2+} from solution using WO_x/C networks. Pb^{2+} tends to be precipitated at high pH as it forms complexes with hydroxide ions. In this work, pH value of ~5was chosen as the initial pH for Pb^{2+} adsorption tests.

The effects of foreign cations on adsorption efficiency were further investigated at pH ~5 in the presence of common competing cations (Na^+ and Ca^{2+}). As shown in Figure S5B, upon addition of Na^+, no significant change in the adsorption capacity canbe observed over the concentration of Na^+ ranging from 0.001 to 0.1 M. By contrast, the presence of Ca^{2+} can slightly reducethe Pb^{2+} adsorption capacity. The decrease of adsorption capacity upon addition of Ca^{2+}, nevertheless, it should be noted that the WO_x/C networks still showed a considerably high adsorption capacity for Pb^{2+}, even when the high concentrationCa^{2+}.The result suggests that the coordination interaction between Pb^{2+} and WO_x/C networks is considerably strong, so these foreign cations cannot well compete with Pb^{2+} ions for the adsorption sites of WO_x/C. These results also reveal that the novel WO_x/C adsorbent should be considerably promising in

capturing Pb^{2+} ions from interfering ions-containing aqueous solution.

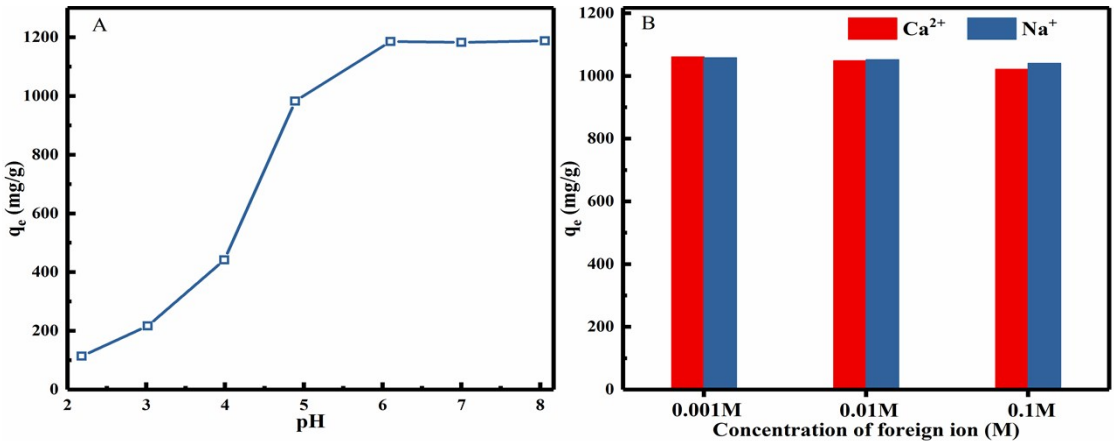

Figure S5. (A) Effect of pH on the adsorption of Pb^{2+} by the WO_x/C networks (initial Pb^{2+}concentration: 120 mg/L, time: 24 h, $NaNO_3$concentration: 0.01 M, 0.1 g/L sorbent); (B) Effect of ionic strength on the adsorption of Pb^{2+} by the WO_x/C networks (initial Pb^{2+} concentration: 120 mg/L, time: 24 h, pH ~5, 0.1 g/L sorbent).

As shown in Figure S6, the removal of Pb^{2+} was slightly reduced by the existence of MB at low initial Pb^{2+} concentrations, and was significantly enhanced by the existence of MB at high Pb^{2+} concentrations in the binary systems. This synergic effect could be explained as follows: there are specific and different active sites for the removal of Pb^{2+} and MB on the WO_x/C networks, and then the appearance of MB on the surface of the WO_x/C networks would offer additional nitrogen and sulfur-containing groups, which might provide new active sites for capturing Pb^{2+}. However, the removal of dyes was not enhanced by the presence of Pb^{2+} for binary systems at similar conditions. One reasonable explanation could be due to that the presence of Pb^{2+} on the surface of the WO_x/C networks could not provide extra active sites for the removal of dyes, leading to the competition for the available removal sites.

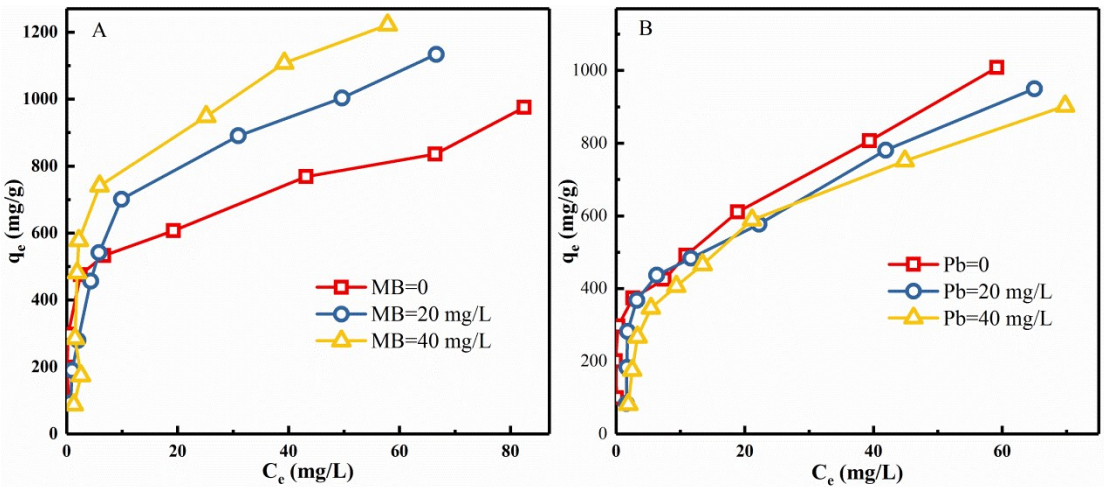

Figure S6. The removal of Pb^{2+} and MB on the WO_x/C networks using binary solutions.

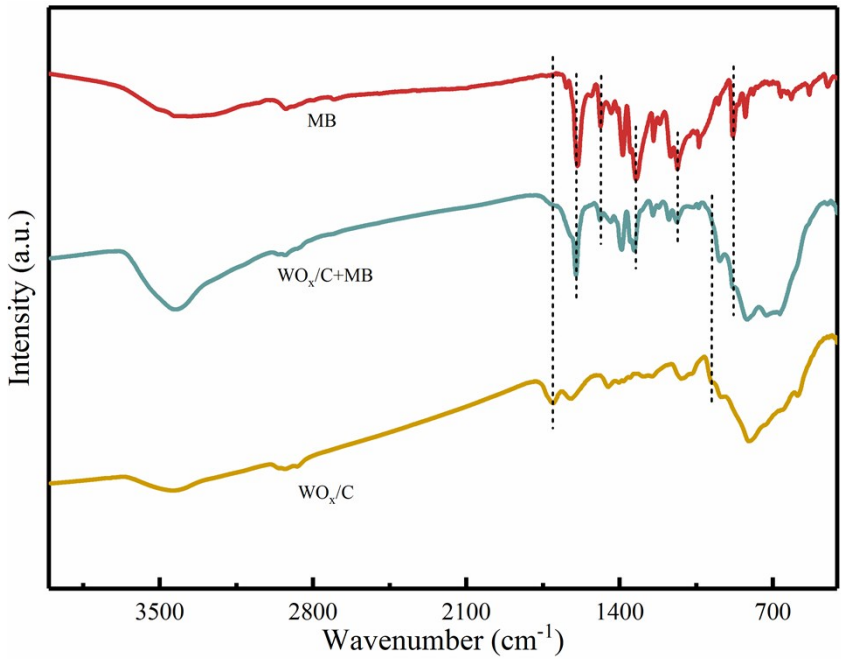

Figure S7. FTIR spectra of WO_x/C before and after MB adsorption.

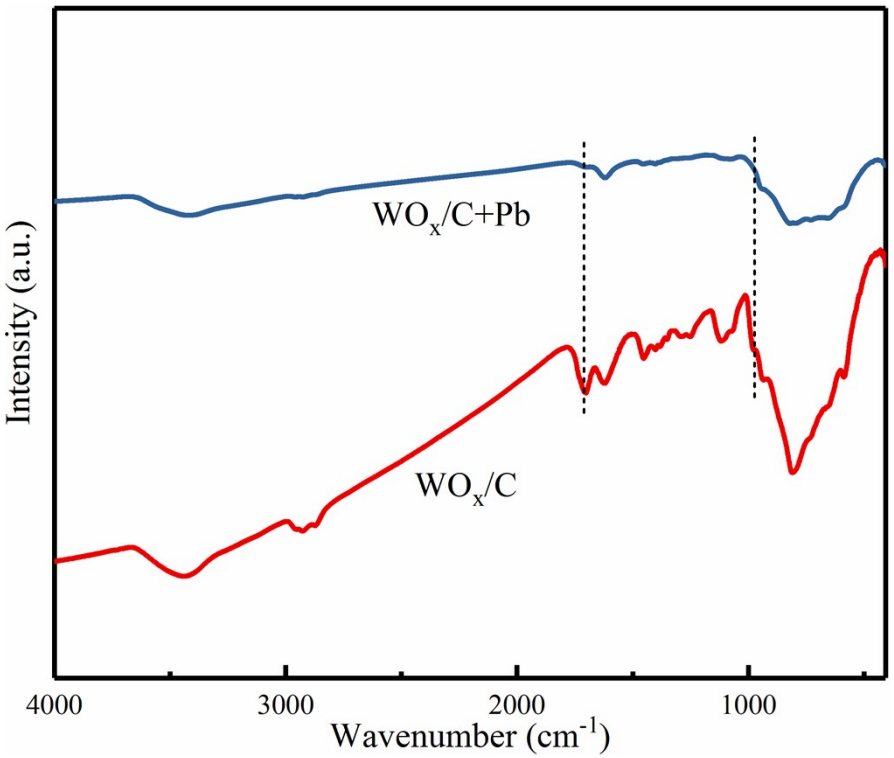

Figure S8. FTIR spectra of WO_x/C before and after Pb^{2+} adsorption.

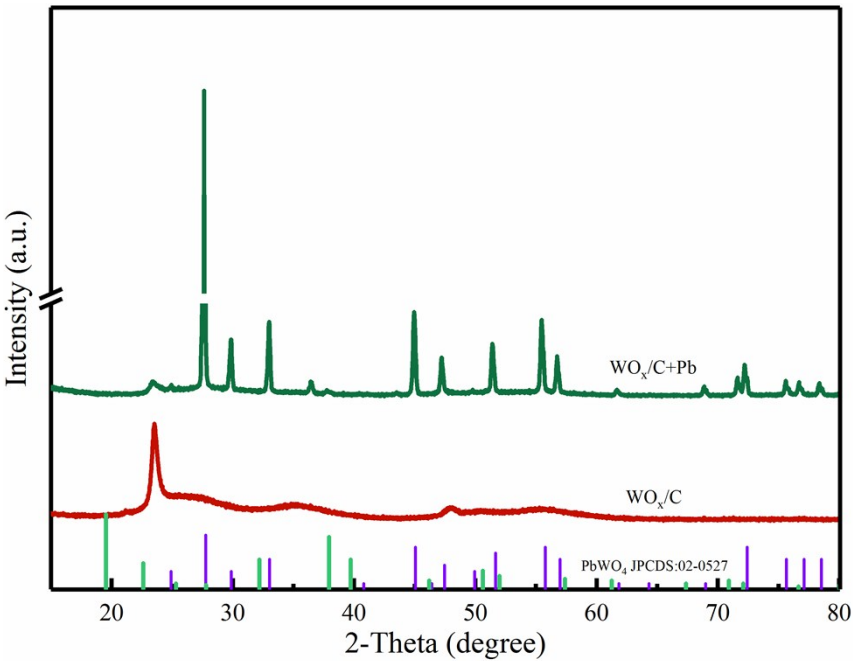

Figure S9. XRD patterns of WO_x/C before and after Pb^{2+} adsorption.

Table S1. Parameters for the kinetic adsorption data fitted by pseudo-first-order and pseudo-second-order models.

Adsorbents	Adsorbate	$q_{e,exp}$ mg/g	Pseudo-first-order			Pseudo-second-order		
			K_1 min^{-1}	$q_{e,cal1}$ mg/g	R^2	K_2 g/mg/min	$q_{e,cal2}$ mg/g	R^2
WO_x	Pb^{2+}	570.64	2.29	604.73	0.997	3.27×10^{-5}	561.07	0.992
	MB	469.57	2.34	500.11	0.998	2.33×10^{-5}	465.84	0.992
WO_x/C	Pb^{2+}	773.19	4.86	782.19	0.999	1.31×10^{-4}	768.95	0.997
	MB	618.24	5.21	627.85	0.998	9.86×10^{-5}	617.57	0.998

Table S2. Parameters of Langmuir and Freundlich models for adsorption of Pb^{2+} and MB onto WO_x and WO_x/C.

Adsorbents	Adsorbate	Langmuir isotherm constants			Freundlich isotherm constants		
		q_m mg/g	K_L L/min	R^2	K_F $mg^{1-1/n}/L^{1/n}/g$	$1/n$	R^2
WO_x	Pb^{2+}	628.88	0.12	0.984	39.19	0.23	0.917
	MB	562.17	0.17	0.944	77.51	0.21	0.951
WO_x/C	Pb^{2+}	1078.83	0.14	0.823	61.55	0.27	0.961
	MB	1301.21	0.06	0.825	85.16	0.36	0.959